論文 / 著書情報
Article / Book Information

論題(和文)	
Title(English)	Influence of wind direction on fatigue damage of seismic isolation dampers
著者(和文)	銭 暁鑫, 佐藤 大樹
Authors(English)	Xiaoxin Qian, Daiki Sato
出典(和文)	, , , pp. 76-83
Citation(English)	Proceedings of the 6th Joint Workshop on Building / Civil Engineering between Tokyo Tech & Tongji, , , pp. 76-83
発行日 / Pub. date	2019, 5

The 6th Joint Workshop on Building / Civil Engineering between Tokyo Tech & Tongji
May 31 – June 1, 2019, Tongji University, Shanghai, China

INFLUENCE OF WIND DIRECTION ON FATIGUE DAMAGE OF SEISMIC ISOLATION DAMPERS

Xiaoxin Qian[1)] , Daiki Sato[2)]

1) Graduate Student, Department of Architecture and Building Engineering, Tokyo Institute of Technology, Japan
2) Associate Professor, Laboratory for Future Interdisciplinary Research of Science and Technology, Tokyo Institute of Technology, Japan

Abstract: Seismic isolation system proves to be efficient in reducing the seismic response of a building. With the increasing number of base-isolated high-rise buildings, the wind effect cannot be neglected. However, only a few people have set foot in the wind-resistant design of base-isolated high-rise buildings. Strong wind may bring about continuous and violent vibration of the flexible isolation layer, leading to the fatigue damage of steel dampers that were installed in the seismic isolation layer. Thus, fatigue damage evaluation is of critical importance to damper performance in the practical design. Previous study aims to investigate the wind-induced response characteristic of the 20-story high-rise seismic isolated steel building constructed at Tokyo Institute of Technology based on the observed records. This current paper focuses on investigating the fatigue damage by means of typhoon simulation. Variations in the fatigue damage degree are observed, and they are summarized according to different cases of wind direction. The authors also evaluate the influence of wind direction by plotting the wind-induced responses of analytical models and residual deformation of isolation layer.

1. INTRODUCTION

It was reported that the 1995 Great Hanshin earthquake shook Japan with historic strength, in which up to more than 6000 people lost their lives and countless buildings were destroyed. From then on, more and more people attempted to set foot in the field of seismic isolation system to ensure that the upper structure is intact in the event of great earthquake. With the recent rapid development of technology, the seismic isolation system is being actively applied to high-rise buildings to meet the demands for people. However, as the structure gets taller, the base-isolated building gradually shows its weakness against strong wind such as typhoon. Unlike earthquake load, wind load tends to increase with height and the strong wind may last long. Therefore, strong wind may bring about continuous and violent vibration of the flexible isolation layer, which may lead to the fatigue damage of steel dampers installed in the isolation layer. Current wind-resistant design of buildings stipulates that buildings should be designed on the assumption that the structure frames and components behave elastically in strong wind. However, as for a base-isolated high-rise building, the seismic isolation layer with long natural period may easily behave plastically. Thus, fatigue damage evaluation of steel dampers is of critical importance to damper performance in the practical design.

Previous study[1] aims to investigate the wind-induced response characteristics of the 20-story base-isolated high-rise building constructed at Tokyo Institute of Technology based on the observed records. Moreover, the study[2] on effects of building aspect ratio on wind-induced responses of based-isolated high-rise buildings and fatigue damage of seismic isolation dampers by time history analysis has been investigated. The results show that the wind-induced responses and fatigue damage degree will decrease as building aspect ratio decreases. However, the study was conducted under the fixed wind direction rather than variable wind direction. The influence of wind direction on wind-induced responses and fatigue damage degree has not been studied yet. Thus, the current paper focuses on investigating the wind-induced responses of base-isolated high-rise buildings and the fatigue damage of seismic isolation dampers by means of time history analysis considering wind direction. Variations in wind-induced responses and fatigue damage are observed, and they are summarized according to two cases of wind direction (fixed wind direction and variable wind direction). In addition, it is considered that wind direction may have great influence on residual deformation of isolation layer. So the authors also evaluate the influence of wind direction by plotting the residual deformation of isolation layer.

The paper is organized as follows: Section 2 presents the analytical model and relevant structural characteristics such as story mass and story stiffness. The explanation on average wind speed and wind direction is described in Section 3. The evaluation of maximum wind responses of analytical models and residual deformation of seismic isolation layer is presented in Section 4. The evaluation of fatigue damage degree (D value) of seismic isolation dampers is also presented in this section. Finally, conclusions and related remarks are given in Section 5.

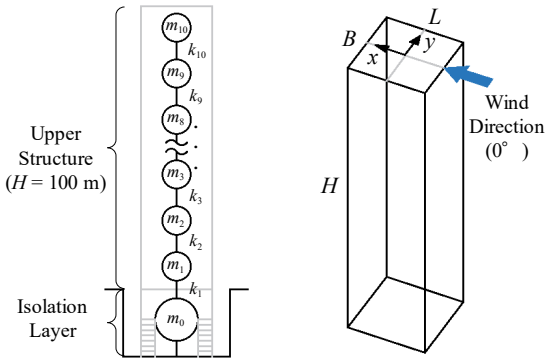

Fig. 1 11-story analytical model

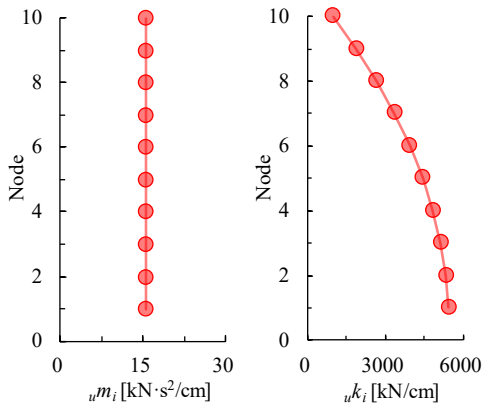

Fig. 2 Characteristics of upper structure

Table 1 Parameters of the analytical model

Aspect ratio (a)		4	[-]
Width (B)		25	[m]
Length (L)		25	[m]
Height (H)		100	[m]
Upper structure	Density (ρ_u)	250	[kg/m^3]
	Natural period (T_u)	2.5	[s]
	Damping ratio (h)	2.0	[%]
Isolation layer	Areal density (ρ_0)	3644	[kg/m^2]
	Natural period (T_0)	6.0	[s]
Yield shear force coefficient of steel damper (α_{dy})		0.03	[-]

Table 2 Characteristics of each story

Aspect ratio		a = 4	
i		m_i [kN·s^2/cm]	k_i [kN/cm]
Upper structure	10	15.6	986.96
	9	15.6	1875.22
	8	15.6	2664.79
	7	15.6	3355.67
	6	15.6	3947.84
	5	15.6	4441.32
	4	15.6	4836.11
	3	15.6	5132.19
	2	15.6	5329.59
	1	15.6	5428.28
Isolation layer	0	22.8	2076.09

2. OUTLINE OF ANALYTICAL MODEL

As shown in Fig. 1, the base-isolated high-rise building is molded to have 11 lumped nodes (or stories). The mass of each node (story) of upper structure is indicated by m_1 to m_{10} while the seismic isolation layer is indicated by m_0. In this paper, the size of building is assumed as H = 100 m, B = 25 m, L = 25 m. So the building aspect ratio is a = 4. As indicated in Table 1, The parameters used in the analysis are: for the upper structure, mass density ρ_u = 250 kg/m^3, natural period T_u = 2.5 s and damping ratio h = 2.0%, while for the isolation layer, areal density ρ_i = 3644 kg/m^2, natural period T_i = 6.0 s and the yield shear force coefficient of overall steel dampers α_{dy} = 0.03. In addition, the wind direction along the x-axis is defined as θ = 0° as shown in Fig. 1.

The 1st mode of vibration is assumed as a straight line. The mass of each story ${}_um_i$ and stiffness of each story ${}_uk_i$ of the upper structure are plotted in Fig. 2 according to the computational results indicated in Table 2. The stiffness of each story ${}_uk_i$ of upper structure can be expressed by Eq. (1) [3].

$$ {}_uk_i = \frac{{}_{us}\omega^2 \cdot m_i \cdot {}_{us}\phi_i + {}_uk_{i+1}({}_{us}\phi_{i+1} - {}_{us}\phi_i)}{{}_{us}\phi_i - {}_{us}\phi_{i-1}} \qquad (1) $$

where, ${}_{us}\omega$ = the natural frequency of 1st mode of upper structure and ${}_{us}\phi_i$ = the 1st mode spectrum of each story of upper structure. However, ${}_uk_{11} = 0$ and ${}_{us}\phi_0 = 0$.

The Restoring force characteristics of overall dampers, isolators and whole isolation layer are shown in Fig. 3. And the characteristics of isolation layer are decided by Eq. (2) ~ (4).

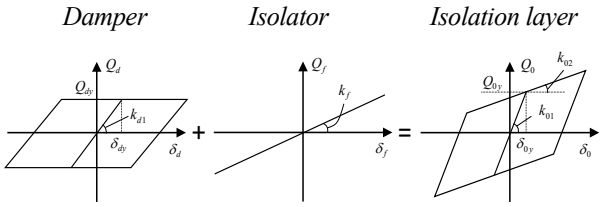

Fig. 3 Restoring force characteristics of isolation layer

$$ k_{d1} = Q_{dy}/\delta_{dy} \qquad (2) $$

$$ Q_{dy} = (W_u + W_b)\cdot\alpha_{dy} \qquad (3) $$

$$ k_f = \frac{4\pi^2(W_u + W_b)}{{}_1T_0^2 \cdot g} \qquad (4) $$

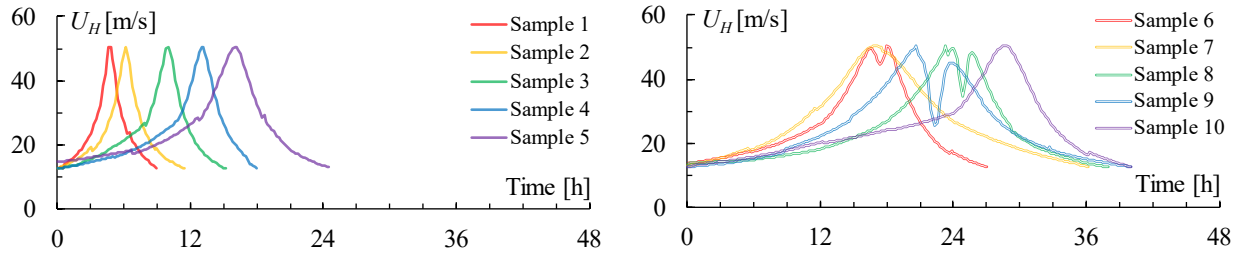

(a) S500 (b) L500

Fig. 4 Average wind speed of typhoon samples

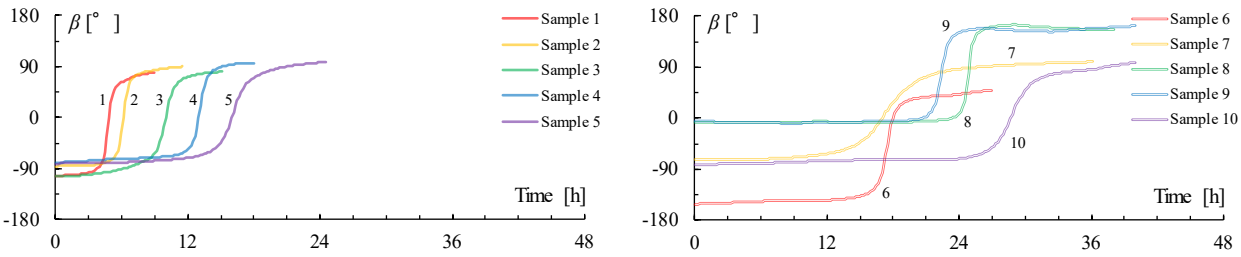

(a) S500 (b) L500

Fig. 5 Wind direction of T_000 before replacement

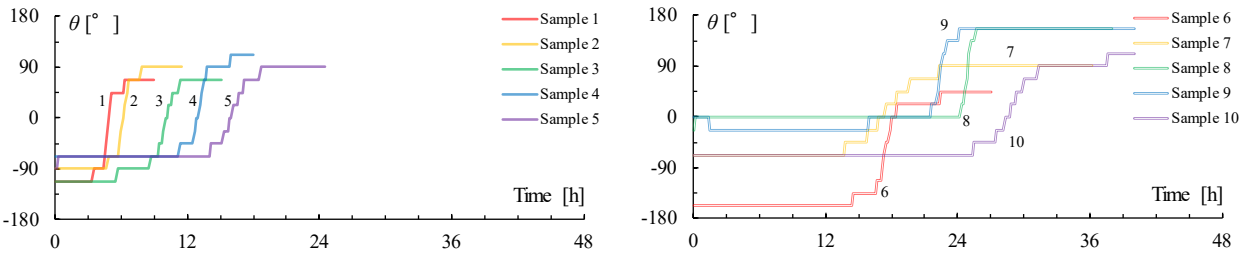

(a) S500 (b) L500

Fig. 6 Wind direction of T_000 after replacement

where, Q_{dy} = the yield capacity of seismic isolation damper, k_{d1} = the initial stiffness of isolation damper, δ_{dy} = yield deformation of seismic isolation damper (assumed as 2.8 cm), α_{dy} = the yield shear force coefficient of seismic isolation damper (assumed as 0.03), k_f = the 1st stiffness of isolators, g = the acceleration of gravity (assumed as 9.81 m/s^2).

By using above computing result, we may get the 1st stiffness k_{01}, 2nd stiffness k_{02} and yield capacity Q_{0y} by Eq. (5) ~ (7) as shown below.

$$k_{01} = k_{d1} + k_f \tag{5}$$

$$k_{02} = k_f \tag{6}$$

$$Q_{0y} = k_{01} \cdot \delta_{dy} \tag{7}$$

3. OUTLINE OF TYPHOON SAMPLES

As shown in Fig. 4, a total of 10 assumed typhoon samples are adopted in the typhoon simulation [4], which are divided into group S500 and group L500 depending on the duration of typhoon. The horizontal axis indicates the duration of typhoon (in hours) and the vertical axis indicates the average wind speed at 100 m above ground U_H (in m/s). The maximum average wind speed ($U_{H,\max}$ = 50.41 m/s) of each typhoon sample is assumed as the 500-year-recurrence wind speed in Tokyo. In addition, each typhoon sample randomly generates 5 waves used for the time history analysis.

In regard to the direction of wind, the time history analysis was carried out considering 2 cases of wind direction, A_000 and T_000. A_000 indicates that the wind direction will not change with the constant wind direction θ = 0°. T_000 indicates that the wind direction will change as shown in Fig. 5. However, as the average wind speed reaches maximum, the wind direction will be fixed at θ = 0°.

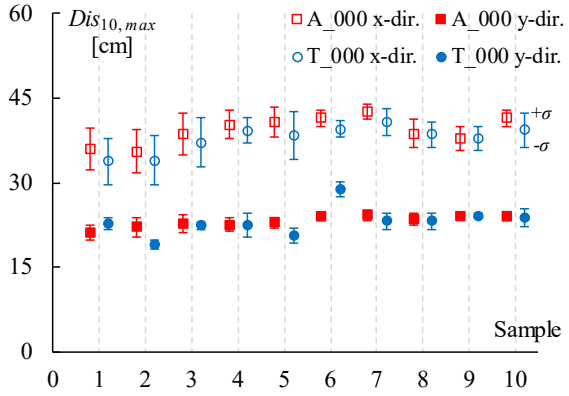

Fig. 7 Max. displacement at 10th story

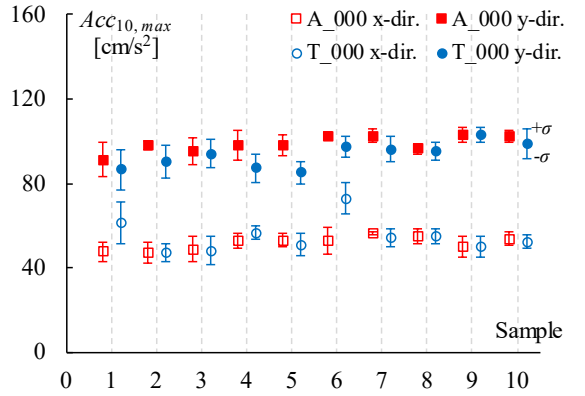

Fig. 8 Max. acceleration at 10th story

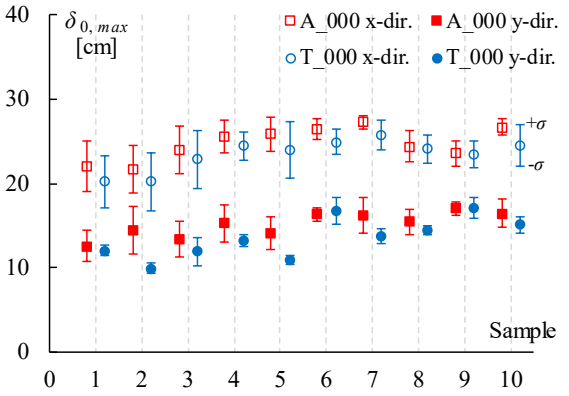

Fig. 9 Max. deformation of isolation layer

Moreover, the wind tunnel experiment was carried out only by the wind direction $\theta = 0°, 22.5°, 45°$ along the x-axis and y-axis, respectively. Therefore, in order to simplified the setting of wind direction in analysis, the analytical wind direction of each sample has been replaced according to experimental wind direction $\theta = 0°, 22.5°, 45°$ as shown in Fig. 6.

4. ANALYTICAL RESULTS

This section will present the results of time history analysis such as the wind-induced responses of analytical models, residual deformation of isolation layer and fatigue damage degree of seismic isolation dampers. The evaluation will be conducted on the basis of the average of 5 waves.

Table 3 Max. displacement at 10th story (x-dir.)

Sample	A_000 [cm]		T_000 [cm]	
	$Dis_{10,max}$	SD	$Dis_{10,max}$	SD
1	35.95	3.61	33.76	4.02
2	35.58	3.74	33.97	4.43
3	38.66	3.65	37.16	4.36
4	40.34	2.59	39.22	2.19
5	40.83	2.69	38.41	4.29
6	41.43	1.57	39.55	1.56
7	42.59	1.37	40.74	2.33
8	38.75	2.55	38.49	2.36
9	37.77	2.05	37.77	2.05
10	41.42	1.51	39.31	3.13

Table 4 Max. acceleration at 10th story (y-dir.)

Sample	A_000 [cm/s^2]		T_000 [cm/s^2]	
	$Acc_{10,max}$	SD	$Acc_{10,max}$	SD
1	91.22	8.12	86.71	9.51
2	98.09	1.82	90.32	8.01
3	95.47	6.42	94.04	6.62
4	98.14	7.16	87.32	6.69
5	98.20	4.96	85.03	5.29
6	102.44	1.70	97.48	5.09
7	102.62	3.34	96.27	6.07
8	96.51	2.31	95.18	4.21
9	102.80	3.49	102.80	3.49
10	102.36	2.53	98.92	6.94

Table 5 Max. deformation of isolation layer (x-dir.)

Sample	A_000 [cm]		T_000 [cm]	
	$\delta_{0,max}$	SD	$\delta_{0,max}$	SD
1	22.07	2.98	20.25	3.12
2	21.77	2.83	20.24	3.45
3	24.04	2.83	22.86	3.40
4	25.58	1.91	24.50	1.65
5	25.92	2.04	23.95	3.33
6	26.45	1.24	24.94	1.49
7	27.33	0.81	25.75	1.75
8	24.44	1.84	24.10	1.72
9	23.57	1.48	23.50	1.57
10	26.69	0.98	24.56	2.50

4.1 Wind-induced responses of analytical models

The maximum displacement and maximum acceleration of 10th story, $Dis_{10,max}$ and $Acc_{10,max}$ from sample 1 to sample 10 are plotted in Fig. 7, 8 and indicated table 3, 4, respectively. From the analytical results of maximum displacement (Fig. 7 and Table 3), it can be seen that the value in x-direction is larger than y-direction. In addition, there is no obvious change in maximum displacement from sample 1 to sample 10. By comparing A_000 with T_000, it is found that the values of A_000 are approximately equal to T_000, for the reason that the duration of typhoon is the same, and when the average wind

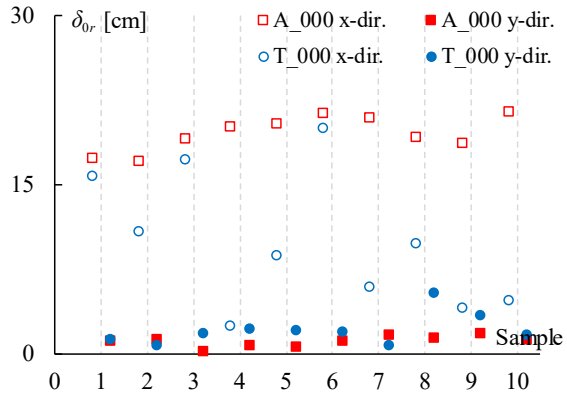

Fig. 10 Residual deformation of isolation layer

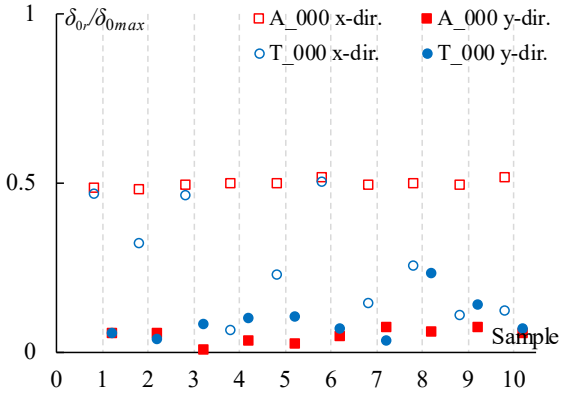

Fig. 11 Residual deformation / Max. deformation

speed reaches maximum, the wind direction is the same as well. So we can obtain the conclusion that the influence of wind direction on maximum displacement is little.

From the analytical results of maximum acceleration (Fig. 8 and Table 4), it can be seen that the value in *y*-direction is larger than *y*-direction. In addition, there is no obvious change in maximum acceleration from sample 1 to sample 10. By comparing A_000 with T_000, it is found that the values of A_000 are approximately equal to T_000 as well except for sample 1 and 6. For the reason that sample 6 has 2 peaks in average wind speed, and when the average wind speed reaches the 2nd peak, the wind direction is fixed along the *y*-direction just in time, which may lead to a larger acceleration along the *x*-axis. However, reason of sample 1 has not been found because sample 1 only has one peak in average wind speed. In a word, we can obtain the similar conclusion that the influence of wind direction on acceleration is little in most case.

The maximum deformation of isolation layer is plotted in Fig. 9 and indicated in Table 5. it can be seen that the value in *x*-direction is larger than *y*-direction. In addition, there is no obvious change in maximum displacement from sample 1 to sample 10. By comparing A_000 with T_000, it is found that the values of A_000 are approximately equal to T_000 like Fig. 7. Similarly, we can obtain the conclusion that the influence of wind direction on maximum deformation of isolation layer is little.

Table 6 Residual deformation of isolation layer (*x*-dir.)

Sample	A_000 [cm]		T_000 [cm]	
	δ_{0r}	*SD*	δ_{0r}	*SD*
1	17.44	2.70	15.80	0.39
2	17.15	2.50	10.93	0.61
3	19.13	2.45	17.27	0.25
4	20.24	1.43	2.55	0.44
5	20.45	1.92	8.80	0.68
6	21.38	1.09	20.04	1.01
7	21.02	0.50	5.90	0.84
8	19.32	0.97	9.85	1.14
9	18.79	1.34	4.12	1.19
10	21.48	0.84	4.81	0.72

Table 7 Residual deformation / Max. deformation (*x*-dir.)

Sample	A_000 [cm]		T_000 [cm]	
	$\delta_{0r}/\delta_{0,\max}$	*SD*	$\delta_{0r}/\delta_{0,\max}$	*SD*
1	0.79	0.02	0.78	0.02
2	0.79	0.01	0.55	0.06
3	0.79	0.01	0.76	0.03
4	0.79	0.01	0.11	0.06
5	0.79	0.02	0.37	0.07
6	0.81	0.00	0.80	0.01
7	0.77	0.02	0.23	0.04
8	0.79	0.02	0.41	0.04
9	0.80	0.01	0.18	0.02
10	0.80	0.00	0.20	0.02

To sum up, the change of wind direction has little effects on maximum displacement at 10th story, maximum acceleration at 10th story and maximum deformation of isolation layer in most cases.

4.2 Residual deformation of seismic isolation layer

Fig. 10 and table 6 show the residual deformation of the seismic isolation layer δ_{0r}. Fig. 11 and table 7 show the ratio of the seismic isolation layer residual deformation δ_{0r} to the seismic isolation layer maximum deformation $\delta_{0,\max}$. From the results of residual deformation (Fig. 10 and table 6), for A_000, there is no obvious change in residual deformation of isolation layer from sample 1 to sample. On the other hand, for T_000, we can see the obvious change. By comparing A_000 with T_000, it is found that, in *x*-direction, the values of T_000 are much smaller than those of A_000 in sample 2, 5, 7, 8, 9, 10. And in *y*-direction, the values of T_000 are much larger than those of A_000 in sample 3, 4, 5, 8, 9. In section 4.1, we got the conclusion that the change of wind direction has little effect on maximum displacement at 10th story, maximum acceleration at 10th story and maximum deformation of isolation layer. However, as for the residual deformation of seismic isolation layer, we can see that the influence of wind direction is great. From the results of the ratio of the seismic isolation layer residual deformation δ_{0r} to the seismic isolation layer maximum deformation $\delta_{0,\max}$, we can get the similar conclusion.

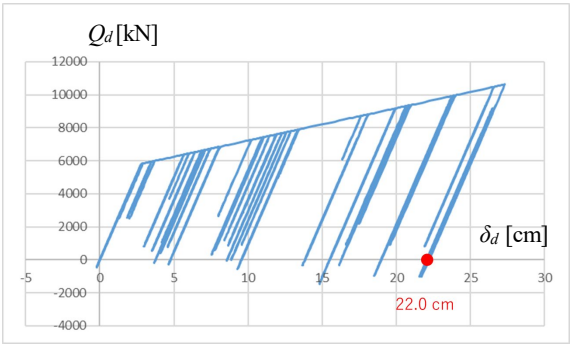

(a) *x*-direction

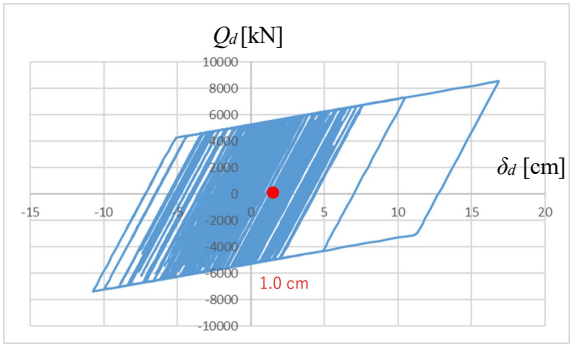

(b) *y*-direction

Fig. 12 Residual deformation of A_000, Sample 2, Wave 1

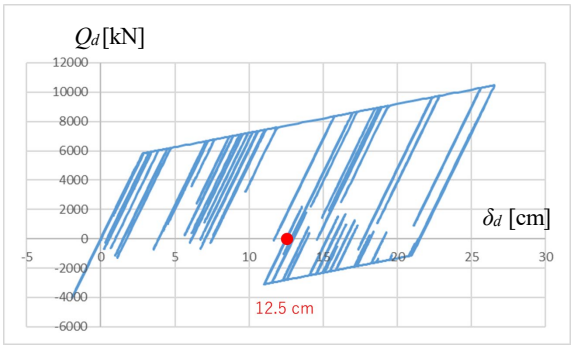

(a) *x*-direction

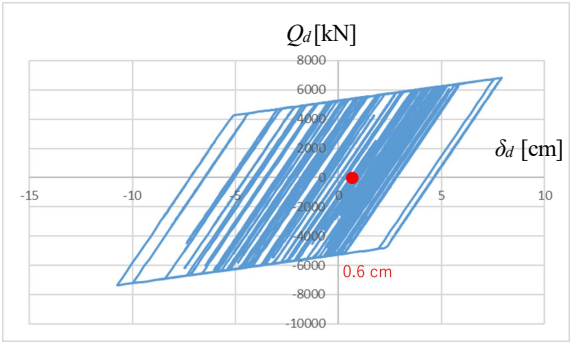

(b) *y*-direction

Fig. 13 Residual deformation of T_000, Sample 2, Wave 1

Table 8 Residual deformation of seismic isolation layer

Unit: cm		A_000								T_000							
Sample	Dir.	wave 1	wave 2	wave 3	wave 4	wave 5	Ave.	SD	CV	wave 1	wave 2	wave 3	wave 4	wave 5	Ave.	SD	CV
1	*x*	16.4	19.9	19.9	12.7	18.3	17.4	2.7	0.2	18.6	19.3	14.9	11.5	14.8	15.8	2.8	0.2
	y	1.6	1.0	1.1	0.6	1.7	1.2	0.4	0.3	2.1	0.2	3.2	0.1	0.6	1.3	1.2	1.0
2	*x*	22.0	15.4	16.5	15.3	16.5	17.1	2.5	0.1	12.5	10.1	10.8	11.4	9.8	10.9	1.0	0.1
	y	1.0	0.7	2.2	1.8	0.7	1.3	0.6	0.5	0.6	0.9	1.6	0.6	0.1	0.8	0.5	0.7
3	*x*	21.7	18.1	16.2	17.3	22.4	19.1	2.4	0.1	20.1	16.0	16.2	14.9	19.3	17.3	2.0	0.1
	y	0.2	0.1	0.7	0.1	0.0	0.2	0.3	1.1	0.9	3.2	1.4	1.4	2.3	1.8	0.8	0.4
4	*x*	20.9	17.6	20.8	21.7	20.2	20.2	1.4	0.1	4.3	3.9	2.8	0.9	0.8	2.5	1.4	0.6
	y	1.3	1.4	0.3	0.6	0.5	0.8	0.4	0.5	1.4	1.7	2.6	2.5	3.0	2.3	0.6	0.3
5	*x*	19.0	18.3	22.6	22.9	19.5	20.4	1.9	0.1	7.8	9.4	10.5	7.8	8.4	8.8	1.0	0.1
	y	0.2	0.6	1.9	0.1	0.2	0.6	0.7	1.2	2.9	1.4	2.8	2.7	1.0	2.2	0.8	0.4
6	*x*	22.2	23.0	20.8	19.9	21.0	21.4	1.1	0.1	20.5	21.7	19.8	17.6	20.5	20.0	1.4	0.1
	y	0.2	2.7	2.0	0.3	0.5	1.1	1.0	0.9	1.8	1.1	1.2	4.0	2.0	2.0	1.0	0.5
7	*x*	20.6	20.7	21.1	20.8	22.0	21.0	0.5	0.0	5.6	7.7	4.7	5.4	6.1	5.9	1.0	0.2
	y	1.2	3.3	1.8	1.7	0.8	1.8	0.8	0.5	0.3	0.6	1.1	0.1	1.7	0.8	0.6	0.7
8	*x*	19.8	19.3	17.8	18.9	20.8	19.3	1.0	0.1	9.7	8.5	8.6	9.5	12.9	9.8	1.6	0.2
	y	1.3	0.2	3.6	1.5	0.8	1.5	1.1	0.8	5.4	6.1	5.3	4.9	5.2	5.4	0.4	0.1
9	*x*	17.0	17.8	19.7	18.8	20.8	18.8	1.3	0.1	4.1	3.5	3.7	3.9	5.4	4.1	0.7	0.2
	y	1.1	1.0	0.6	3.7	2.7	1.8	1.2	0.7	1.9	3.5	4.0	4.3	3.2	3.4	0.8	0.2
10	*x*	21.7	21.4	20.2	22.8	21.4	21.5	0.8	0.0	5.0	5.0	4.8	4.6	4.6	4.8	0.2	0.0
	y	0.2	2.5	1.5	1.2	1.3	1.3	0.7	0.5	1.6	1.2	2.6	1.7	1.2	1.6	0.5	0.3

Table 9 D value

Sample	Case	Wave 1			Wave 2			Wave 3			Wave 4			Wave 5			$D=\Sigma(D_x+D_y)/5$
		D_x	D_y	D_x+D_y	D_x	D_y	D_x+D_y	D_x	D_y	D_x+D_y	D_x	D_y	D_x+D_y	D_x	D_y	D_x+D_y	
1	A_000	0.01	0.08	0.09	0.01	0.08	0.09	0.01	0.09	0.10	0.01	0.08	0.09	0.01	0.09	0.10	0.09
	T_000	0.02	0.03	0.04	0.02	0.02	0.04	0.02	0.03	0.05	0.02	0.02	0.04	0.01	0.03	0.04	0.04
2	A_000	0.01	0.08	0.10	0.01	0.08	0.09	0.01	0.09	0.10	0.01	0.09	0.10	0.01	0.10	0.10	0.10
	T_000	0.01	0.04	0.05	0.01	0.03	0.03	0.01	0.03	0.03	0.01	0.02	0.03	0.01	0.03	0.04	0.04
3	A_000	0.02	0.14	0.15	0.01	0.13	0.15	0.01	0.13	0.14	0.01	0.13	0.14	0.01	0.12	0.13	0.14
	T_000	0.02	0.06	0.07	0.01	0.06	0.07	0.01	0.06	0.07	0.01	0.05	0.06	0.02	0.05	0.07	0.07
4	A_000	0.02	0.13	0.14	0.01	0.12	0.14	0.02	0.14	0.16	0.02	0.15	0.17	0.01	0.13	0.15	0.15
	T_000	0.02	0.05	0.07	0.02	0.04	0.06	0.02	0.05	0.08	0.03	0.06	0.09	0.02	0.05	0.07	0.07
5	A_000	0.02	0.20	0.22	0.02	0.21	0.23	0.03	0.23	0.26	0.03	0.23	0.26	0.02	0.21	0.23	0.24
	T_000	0.02	0.06	0.08	0.01	0.06	0.08	0.02	0.07	0.10	0.03	0.07	0.09	0.02	0.07	0.09	0.09
6	A_000	0.03	0.33	0.36	0.03	0.34	0.38	0.03	0.34	0.37	0.03	0.32	0.36	0.04	0.35	0.39	0.37
	T_000	0.05	0.08	0.13	0.04	0.10	0.14	0.04	0.10	0.14	0.05	0.09	0.14	0.04	0.10	0.15	0.14
7	A_000	0.05	0.48	0.53	0.06	0.48	0.53	0.05	0.49	0.54	0.05	0.48	0.53	0.06	0.52	0.57	0.54
	T_000	0.04	0.14	0.18	0.04	0.14	0.18	0.04	0.14	0.19	0.05	0.14	0.19	0.05	0.15	0.20	0.19
8	A_000	0.03	0.35	0.38	0.03	0.34	0.37	0.03	0.34	0.37	0.03	0.33	0.36	0.04	0.32	0.36	0.37
	T_000	0.03	0.23	0.27	0.03	0.23	0.26	0.03	0.23	0.26	0.03	0.23	0.26	0.04	0.23	0.27	0.26
9	A_000	0.02	0.33	0.36	0.03	0.31	0.33	0.03	0.34	0.37	0.03	0.34	0.37	0.03	0.35	0.37	0.36
	T_000	0.02	0.24	0.27	0.03	0.23	0.26	0.03	0.25	0.28	0.03	0.24	0.27	0.03	0.25	0.28	0.27
10	A_000	0.04	0.34	0.38	0.03	0.33	0.36	0.03	0.31	0.34	0.04	0.34	0.38	0.03	0.34	0.37	0.37
	T_000	0.03	0.10	0.13	0.03	0.09	0.12	0.03	0.09	0.12	0.04	0.11	0.15	0.03	0.10	0.14	0.13

Fig. 12, 13 show the relationship between force and deformation of seismic isolation dampers of one example (sample 2, wave 1). The red points marked in the figure indicate the residual deformation. In addition, the residual deformation of all samples is indicated in Table 8. we can see that the influence of wind direction is great, especially in x-direction.

4.3 Fatigue damage degree of seismic isolation damper

The fatigue damage degree of seismic isolation damper (D value) is calculated by using rain-flow method and Miner's rule, which can be expressed by[5]

$$D=\sum D_k=\sum_{k=1}^{np}\frac{N_k}{N_{f(\delta_k)}} \tag{8}$$

The D values of Sample 1~10 obtained by time history analysis are indicated in Fig. 14 and Table 9. The D value of each wave D_x+D_y can be expressed by the sum of D value in x- and y- directions, D_x and D_y. The final D value of each sample can be expressed by the average of all D_x+D_y.

From the results, it can be seen that D_x is much smaller than D_y. For A_000, the maximum D value is found to occur in Sample 7. In addition, the variation in D values from Sample 1 to 10 is obvious. Thus, D value is greatly affected by duration of typhoon. However, longer duration of typhoon may not lead to larger D value. Both duration of typhoon and average wind speed may influence the final D value. On the other hand, for T_000, the maximum D value is found to occur in Sample 9. By comparing A_000 with T_000, it is found that the D values of all samples decrease compared with A_000, and the ratio is about 1.3 to 2.8 times. Thus, the wind direction has great influence on fatigue damage degree of seismic isolation dampers.

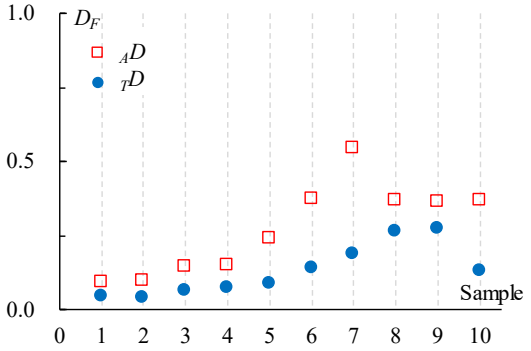

Fig. 14 D value

It is note that the fatigue damage degree is calculated according to fatigue damage curve obtained by fatigue test of seismic isolation dampers. However, the amplitude of tests ranges from 48.6 mm to 374 mm. And in the analysis, most amplitudes are under the 48.6 mm. So the fatigue damage curve with extension has been adopted in the analysis, which may decrease the accuracy in calculation the D value. In order to complement the fatigue damage curve, relevant tests will be carried to obtain a complete fatigue damage curve.

5. CONCLUSIONS

In this paper, we investigated the maximum wind-induced responses of the base-isolated high-rise buildings, residual deformation of seismic isolation layer and the fatigue damage degree of seismic isolation dampers by using typhoon simulation. The results show that the change of wind direction has little effects on maximum displacement at 10^{th} story, maximum acceleration at 10^{th} story and maximum deformation of isolation layer in most cases. However, the change of wind direction has great effects on residual deformation of seismic isolation layer and fatigue damage degree of seismic isolation dampers.

In wind resistant design, the maximum responses of base-isolated high-rise building can be properly evaluated on the safety side by A_000. However, the residual deformation of seismic isolation layer and fatigue damage degree of seismic isolation dampers may be overestimated by A_000. Therefore, it is necessary to consider the change in wind direction in the evaluation of residual deformation and fatigue damage degree.

Since the conclusion given out in this paper is only based on one type of base-isolated high-rise building. It may come to different conclusions when the parameters such as the building shape or natural period of isolation layer changes. Moreover, the results show quite large standard deviations, so it is necessary to increase the number of waves in the further study.

Acknowledgements:

This work was supported by JST Program on Open Innovation Platform with Enterprises, Research Institute and Academia. The authors acknowledge support from Nikken Sekkei Ltd., Izumisohken Engineering Co., Ltd. and Kanagawa University. Special thanks to Nishijima Lab. in Kyoto University for providing precious experimental data of wind tunnel experiment.

References:

[1] Daiki Sato, Tetsuro Tamura, Yoshiyuki Fugo, Osamu Nakamura, Akira Katumura, Kazuhiko Kasai, Haruyuki Kitamura. Wind-induced Response Characteristic Evaluation of High-rise Seismic Isolated Building Based on Observed Records, 14th International Conference on Wind Engineering, Proceedings of the 14th International Conference on Wind Engineering, Jun. 2015.

[2] Xiaoxin Qian, Daiki Sato, Sei Mabashi. Evaluation of Fatigue Damage of Seismic Isolation Dampers by Wind Response Analysis Effects of Building Aspect Ratio on Fatigue Damage Degree, Architectural Institute of Japan, pp. 497-500, 2019.3

[3] D. Sato, K. Kasai and T. Tamura, INFLUENCE OF FREQUENCY SENSITIVITY OF VISCOELASTIC DAMPER ON WIND-INDUCED RESPONSE, Journal of Structural and Construction Engineering (Transactions of AIJ), Vol. 74, No. 635, pp. 75-82. (in Japanese)

[4] N. Danguri and K. Nishijima, Method for Selecting Hazard-Consistent Most-Likely Typhoon Based on Probabilistic Typhoon Model, DPRI Annual Meeting, B19, Feb. 2018. (in Japanese)

[5] T. Murakami, D. Sato, T. Tamura, Y. Fugo, M. Ikegami, K. Yoshie, K. Kasai and H. Kitamura, Fatigue damage evaluation of the steel material damper of High-rise Seismic Isolated Building Based on Observation Data, Journal of Wind Engineering, JAWE, Vol. 40, No. 143, pp. 191-192, Apr. 2015. (in Japanese)

[6] Shoichi Kishiki, Yuta Ohkawara, Satoshi Yamada, akira wada. EXPERIMENTAL EVALUATION OF CYCLE DEFORMATION CAPACITY OF U-SHAPED STEEL DAMPERS FOR BASE ISOLATED STRUCTURES, Journal of Structural and Construction Engineering,Vol. 73, No. 624, pp. 333-340, 2008.2